Photocatalytic degradation of azithromycin formulation in aqueous solution by doped titanium dioxide/fiberglass-rubberized silicone photocatalytic membrane

Giovanina-Iuliana Lupu[1], Cristina Orbeci[1*], Constantin Bobirică[1], Liliana Bobirică[1], Elena Sorana Lazăr[2], Jeanina Pandele-Cusu[2], Marian Nicolae Verziu[3], Cristian Pîrvu[4] and Roberta-Geanina Irodia[4]

Abstract

The objective of this work was to develop a novel photocatalytic membrane for the photocatalytic degradation of azithromycin formulation from aqueous solutions which, in addition to a high photocatalytic activity, should have a good mechanical and physico-chemical stability over time. Thus, the $Nb-TiO_2$ and $Nb-Fe-TiO_2$ photocatalysts were prepared by the solution combustion synthesis method, and then they were manually embedded in a fiberglass – rubberized silicone support. The mineralogical, morphological, and structural characterization of the obtained materials showed that both niobium and iron replace titanium in the titanium dioxide network, thus confirming the synthesis of new photocatalysts. The results of the photocatalytic oxidation tests showed a good photocatalytic activity of the developed photocatalytic membranes (degradation efficiency of up to 70% in the first 15 min of irradiation), this being on the one hand attributed to the increase of the specific surface of the photocatalyst by introducing niobium into the photocatalyst structure, and on the other hand due to the triggering of the Fenton photo oxidation mechanism due to the presence of trivalent iron in the photocatalyst structure. Also, the results indicated an excellent mechanical and physico-chemical resistance of the photocatalytic membranes, they are being practically inert to the harsh conditions in the photocatalytic reactor.

Keywords Photocatalytic membrane, Fiberglass, Rubberized silicone, Niobium doped titanium dioxide, Azithromycin formulation

*Correspondence:
Cristina Orbeci
cristina.orbeci@upb.ro
[1] Department of Analytical Chemistry and Environmental Engineering, National University of Science and Technology Politehnica Bucharest, Bucharest 060042, Romania
[2] "Ilie Murgulescu" Institute of Physical Chemistry, Romanian Academy, Bucharest 060021, Romania
[3] Department of Bioresources and Polymer Science, National University of Science and Technology Politehnica Bucharest, Bucharest 060042, Romania
[4] Department of General Chemistry, National University of Science and Technology Politehnica Bucharest, Bucharest 060042, Romania

1 Introduction

Azithromycin is a broad-spectrum antibiotic from the macrolide class and is heavily used for bacterial infections such as respiratory tract infections, genitourinary infections, or enteric infections [1]. It is eliminated mainly unchanged in feces and urine, which, in turn, end up in municipal wastewater [2]. The chemical structure of azithromycin is illustrated in Fig. 1 [3]. A high organic loading of municipal wastewater with antibiotics such as azithromycin puts a lot of pressure on the biological stage of municipal treatment plants, often requiring their passage through advanced treatment stages such as

Lupu *et al. Sustainable Environment Research*   (2023) 33:36
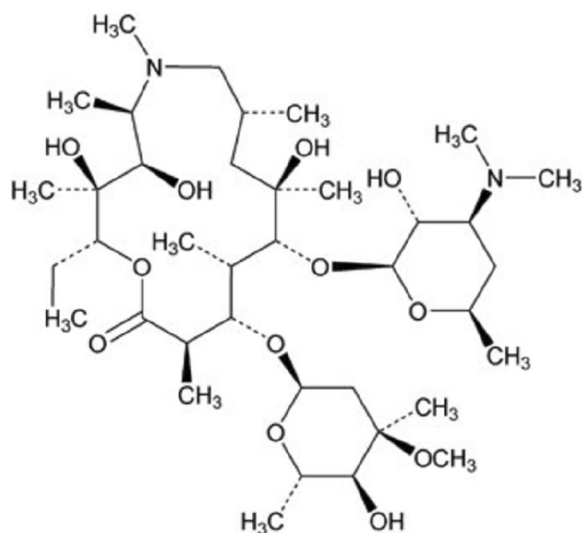
Page 2 of 12

Fig. 1 Chemical structure of azithromycin

retention on various adsorbent materials [4, 5], electro-coagulation [6, 7], advanced oxidation [8, 9], etc. Starting with the 1980s, photocatalysis began to gain increasing interest especially due to the complete and rapid degradation of organic material without generating secondary pollution. Thus, various photocatalytic systems were experimented with a wide range of photocatalysts [10]. Photocatalysts, of which the most used is titanium dioxide (TiO_2) as such or doped with various other elements to increase the photocatalytic activity in certain working conditions, are either used in suspension or immobilized on various supports (deposited on the surface or embedded) such as polymer films, glass fiber nets, glass plates, etc. [11]. Hybrid photocatalytic membranes have also been developed that combine the specific elements of photocatalysis with those of membrane processes in unified treatment method. However, the main issue that can occur is related to membrane fouling [12, 13].

Photocatalytic reactors that use photocatalytic membranes (immobilized photocatalyst) have some advantages compared to suspension photocatalytic reactors (photocatalyst in suspension), such as the elimination of the recovery stage of the photocatalyst from the suspension at the end of the irradiation time, and the possibility of configuring the reactor so that all the photocatalyst is exposed to radiation [14]. Polymer-supported photocatalysts represent one of the most popular types of photocatalytic membranes [15]. The main problem related to this type of photocatalytic membrane is its stability under the working conditions inside the photocatalytic reactor. The highly reactive species generated during irradiation or even UV radiation can damage the polymer support [16]. The degradation of the photocatalytic membrane

leads to the release of both the organic degradation compounds and the contained photocatalyst into the solution. This leads to the reduction of its photocatalytic efficiency and makes it impractical for another irradiation cycle [17].

Therefore, the main objective of this work is to develop a polymer-supported photocatalyst type photocatalytic membrane that has both a high photocatalytic activity for the degradation of antibiotics such as azithromycin from aqueous solutions, and a high mechanical and physico-chemical stability that to make it long-term usable in photocatalytic reactors. The photocatalyst is titanium dioxide doped with niobium (Nb-TiO_2) or titanium dioxide co-doped with niobium and iron (Nb-Fe-TiO_2), which is impregnated in a novel support based on fiberglass and rubberized silicone (fiberglass- rubberized silicone).

2 Material and methods

2.1 Materials

Azitrox formulation, powder for oral suspension, (200 mg azithromycin per 5 mL of reconstituted oral suspension) from Zentiva was purchased from a human pharmacy and used in experimental tests. It contains the active component (azithromycin dihydrate) and a series of organic and inorganic excipients (i.e., sugar, trisodium phosphate anhydrous, hydroxypropyl cellulose, xanthan gum, and banana flavor). Hydrogen peroxide solution of 30% by mass was purchased from Sigma-Aldrich and has the role to be a source of hydroxyl radical species. 1 N solution of sulfuric acid was purchased from Sigma-Aldrich and was used for adjusting the pH of the working solutions. Ti(IV) iso-propoxide (Sigma Aldrich), nitric acid (Sigma Aldrich), glycine (Carl Roth) ammonium niobate(V) oxalate hydrate (Sigma Aldrich), and iron(III) chloride hexahydrate (Sigma Aldrich), were used for the synthesis of photocatalysts without further purification. Pure water was used for preparing all reagents and working solutions.

2.2 Photocatalysts synthesis

Two types of photocatalysts were synthesized by the solution combustion synthesis method, namely niobium doped titanium dioxide (Nb-TiO_2) and niobium-iron co-doped titanium dioxide (Nb/Fe-TiO_2). The first type of photocatalyst has a weight of doped niobium of 15 wt%, while the second type of photocatalyst keeps the same weight of niobium but has two different weights of iron, namely 0.8 and 1.6 wt% Therefore, three different photocatalysts resulted, namely Nb(15 wt%)-TiO_2 coded as P1, Nb(15 wt%)/Fe(0.8 wt%.)-TiO_2 coded as P2, and Nb(15 wt%.)/Fe(1.6 wt%)-TiO_2 coded as P3. The synthesis of these photocatalysts began with the preparation of the oxidant titanyl nitrate by slow hydrolysis of 9 mL Ti(IV)

Lupu *et al. Sustainable Environment Research*　　　(2023) 33:36

Page 3 of 12

iso-propoxide added drop wise under vigorous stirring in 30 mL pure water followed by nitration with 4 mL of nitric acid under ice cold conditions and vigorous stirring for 3 h. Next, to prepare Nb-TiO$_2$ type photocatalyst (P1) the titanyl nitrate obtained was mixed for 1 h under stirring with glycine (2.4 g) and ammonium niobate(V) oxalate hydrate (1.17 g). To prepare Nb/Fe-TiO$_2$ type photocatalysts (P2 and P3), iron(III) chloride hexahydrate (0.1 or 0.2 g) is added to the mixture above. After thorough mixing, the resulting solutions were kept in furnace at 773 K for 1 h. It should be mentioned that TiO$_2$ itself was also prepared by the same procedure, but without adding the niobium and iron salts.

2.3 Preparation of photocatalytic membranes
The three photocatalysts were mixed separately under continuous stirring with a silicone rubber paste (commercial brand) at a silicone rubber/photocatalyst mass ratio of 5/1. Next, fiberglass nets with the dimensions 30 cm (L) × 30 cm (B) were manually immersed in the thin layers of the rubberized silicone - photocatalyst mixtures obtained and preliminarily cast in a thin film in glass trays, and then left to dry at room temperature for 24 h. Later, the membranes were detached from the glass trays and wrapped in a cylindrical shape. Thus, three photocatalytic membranes were prepared, namely Nb(15 wt%)-TiO$_2$/fiberglass-rubberized silicone coded as M1, Nb(15 wt%)/Fe(0.8 wt%)-TiO$_2$/fiberglass-rubberized silicone coded as M2, and Nb(15 wt%)/Fe(1.6 wt%)-TiO$_2$/fiberglass-rubberized silicone coded as M3.

2.4 Photocatalytic degradation experiments
The photocatalytic degradation experiments were taking place in accord to the experimental conditions presented in Table 1. An aqueous stock solution of 0.5 g L^{-1} azithromycin formulation (azithromycin plus excipients) was prepared by dissolving 5 g of Azitrox powder in 10 L of pure water. The stock solution is kept at room temperature for at least 24 h until the experiments are carried out. The aqueous working solution of azithromycin

Table 1 Experimental conditions for the photocatalytic degradation tests

Photocatalytic reactor volume, L	1.5
Recirculation flow rate, L min^{-1}	2.0
Volume of working solution, L	2.0
UV lamp	High-pressure mercury lamp power of 120 W intensity (peak irradiance) of 1.5 mW cm^{-2}
pH of working solution	3
Reaction time, min	120

formulation (azithromycin plus excipients) of 0.02 g L^{-1} was prepared at the beginning of each experiment by diluting 100 mL stock solution of azithromycin formulation in 2.5 L of pure water. This concentration was established to obtain an initial equivalent chemical oxygen demand (COD) of 250 mg L^{-1} by repeated COD measurements. After preparation, the pH of the working solution is adjusted to the working value (pH 3) with 1 N sulfuric acid. Next, the working solution is passed into the photocatalytic reactor, 10 mL of hydrogen peroxide is added at the beginning of the irradiation process to initiate the generation of hydroxyl radicals, and it is further subjected to UV irradiation for 2 h. The UV photocatalytic reactor is equipped with a water-cooling jacket and with an external centrifugal pump which continuously recirculates the working solution through a recirculation vessel. The UV lamp and photocatalytic were coaxially positioned in a reactor. Samples of 10 mL were taken from the reactor at predefined irradiation times (5, 15, 30, 60, 90, and 120 min). Then, the samples were prepared for COD analysis according to the APHA 5220 D Standard Method [18]. It should be noted that, according to the mentioned standard, the calibration curves were obtained by using the standard potassium hydrogen phthalate solution with COD equivalents in the range of 20 to 900 mg L^{-1}. LT 200 digestion unit (Hach Lange GmbH) and DR 3800 spectrophotometer (Hach Lange GmbH) were used in COD analysis.

2.5 Characterization of obtained photocatalysts and photocatalytic membranes
The mineralogical characterization of the photocatalysts was carried out using a Rigaku Ultima IV diffractometer equipped with a Cu Kα monochromatic radiation source (λ = 1.5406 Å) operating at 40 kV and 30 mA. Each diffractogram was recorded in the 10–80° (2θ) range. The results were interpreted using the PDXL programme of the Rigaku diffractometer and the ICDD PDF-2 database. Determination of crystallite sizes was carried out using the Debye−Scherrer equation. Textural characteristics of the photocatalysts were determined using N$_2$ adsorption/desorption isotherms at −196 °C acquired with a Micromeritics ASAP 2020 analyzer. Samples were degassed under vacuum at 300 °C for 4 h prior to measurements. A Quanta 650 FEG scanning electron microscope (SEM) equipped with energy dispersive X-rays (EDX) analyzer operated at 10 kV was used to investigate the morphology of both photocatalysts and photocatalytic membranes. Fourier transform infrared (FTIR) analysis of photocatalysts and photocatalytic membranes was performed on an ATR-FTIR spectrum 100 (PerkinElmer) with 4 consecutive scans in the 4000–550 cm^{-1} region and

Lupu *et al. Sustainable Environment Research*   (2023) 33:36

Page 4 of 12

4 cm^{-1} resolution. The presented spectra are the average of these scans. X-ray Photoelectron Spectroscopy (XPS) was performed for both photocatalysts and photocatalytic membranes by using a K-Alpha instrument with a monochromate Al Kα source which offer photons with 1486.6 eV. Binding energies were calibrated by placing the C 1 s peak at 284.4 eV.

3 Results and discussion

3.1 X-ray diffractometry

The diffraction lines (Fig. 2) at 2θ = 25.1, 37.6, 47.9, 53.5, 54.9 and 62.3° characteristic of the (101), (004), (200), (105), (211) and (204) planes correspond to the pure anatase phase of TiO$_2$ [19]. The lack of any phase segregation of the three oxides (TiO$_2$, Nb$_2$O$_5$ and Fe$_3$O$_4$) was highlighted by the absence of diffraction lines characteristic for niobium or iron oxides [20, 21], suggesting the substitution of Ti^{4+} by niobium and iron ions. On the other hand, the value of ionic radius of Ti^{4+} may depend on its coordination, so that, in the tetrahedral coordination the ionic radius of Ti^{4+} is 0.42 Å and 0.6 Å in that octahedral [22]. The ionic radius of Nb^{5+} is 0.64 Å [23]. Therefore, a substitution between Nb^{5+} is possible, especially with octahedral Ti^{4+}. The incorporation of niobium into anatase structure led to a decrease in crystallinity of the catalyst, as obtained from the Scherrer equation using the highest diffraction lines which correspond to (101) plane: from 8.6 nm of TiO$_2$ to 6.6 nm in P1 and 6.5 nm in P2.

3.2 N$_2$ adsorption/desorption isotherms

The insertion of niobium and iron into TiO$_2$ structure was accompanied by a significant increase of specific surface area while only minor modifications of the pores size were noticed, which is in agreement to the decrease of crystallite size noticed in XRD analysis [24]. The results are presented in Table 2.

3.3 SEM/EDX spectroscopy

The morphology of the photocatalysts is presented in Fig. 3a–c. As can be seen in the SEM images, there are some agglomerated bulks which are maintained in about the same shape and density for all three photocatalysts. The iron peak intensity in EDX spectra increases as the iron amount incorporated into titania structure increases, while the niobium peak intensity is kept constant (EDX spectra in Fig. 3b and c). Therefore, in agreement with XRD analysis, the increase of iron amount inserted suggests a substitution of Ti^{4+} with iron species.

The morphology of the photocatalytic membranes is presented in Fig. 4a–c. As can be seen from Fig. 4a, the photocatalytic membrane M1 shows agglomerations of the photocatalyst (P), which denotes an uneven deposition of it on the surface of the membrane. It seems that, in the case of the M2 and M3 photocatalytic membranes, the photocatalyst is embedded in rubberized silicone (S-R), and the distribution of the photocatalyst (P) in the membrane is much more homogeneous than in the case of the M1 photocatalytic membrane (Fig. 4b and c).
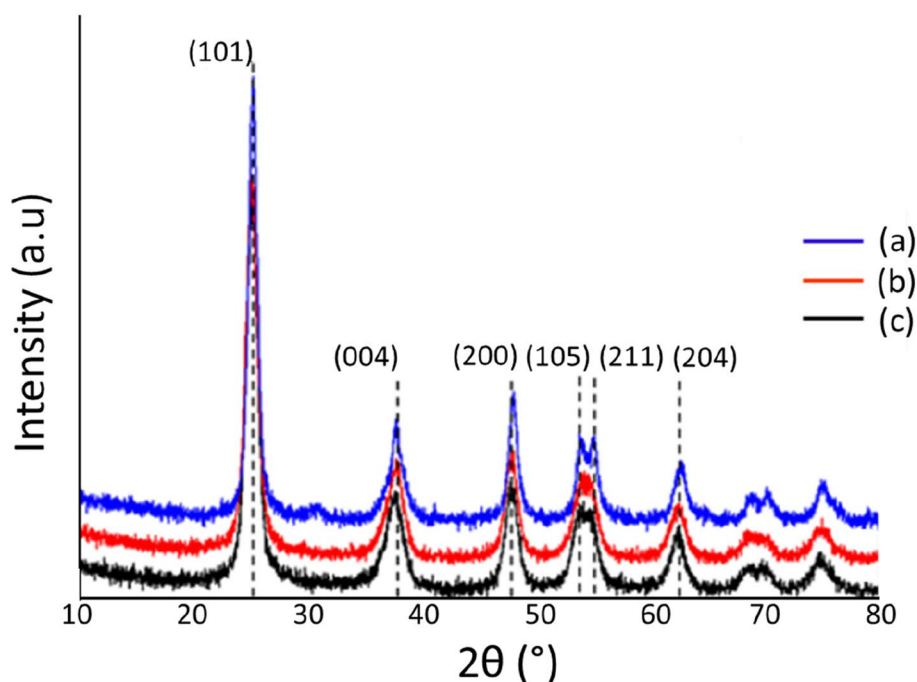

Fig. 2 X-ray diffraction patterns of the prepared catalysts (a) TiO$_2$ (control), (b) P1, (c) P3

Table 2 Textural characteristics of the photocatalysts

Material	Specific surface (m² g⁻¹)	Pore size (nm)
TiO₂ (control)	94	3.8
P1	164	4
P3	151	4

3.4 Infrared spectroscopy

Figure 5a shows the FTIR spectra for all the three initial photocatalysts. The presence of some weak transmittance between 700–730 cm⁻¹ are attributed to the stretching vibrations of the Ti-O groups. All the three spectra show peaks around 1000 cm⁻¹ which could be assigned
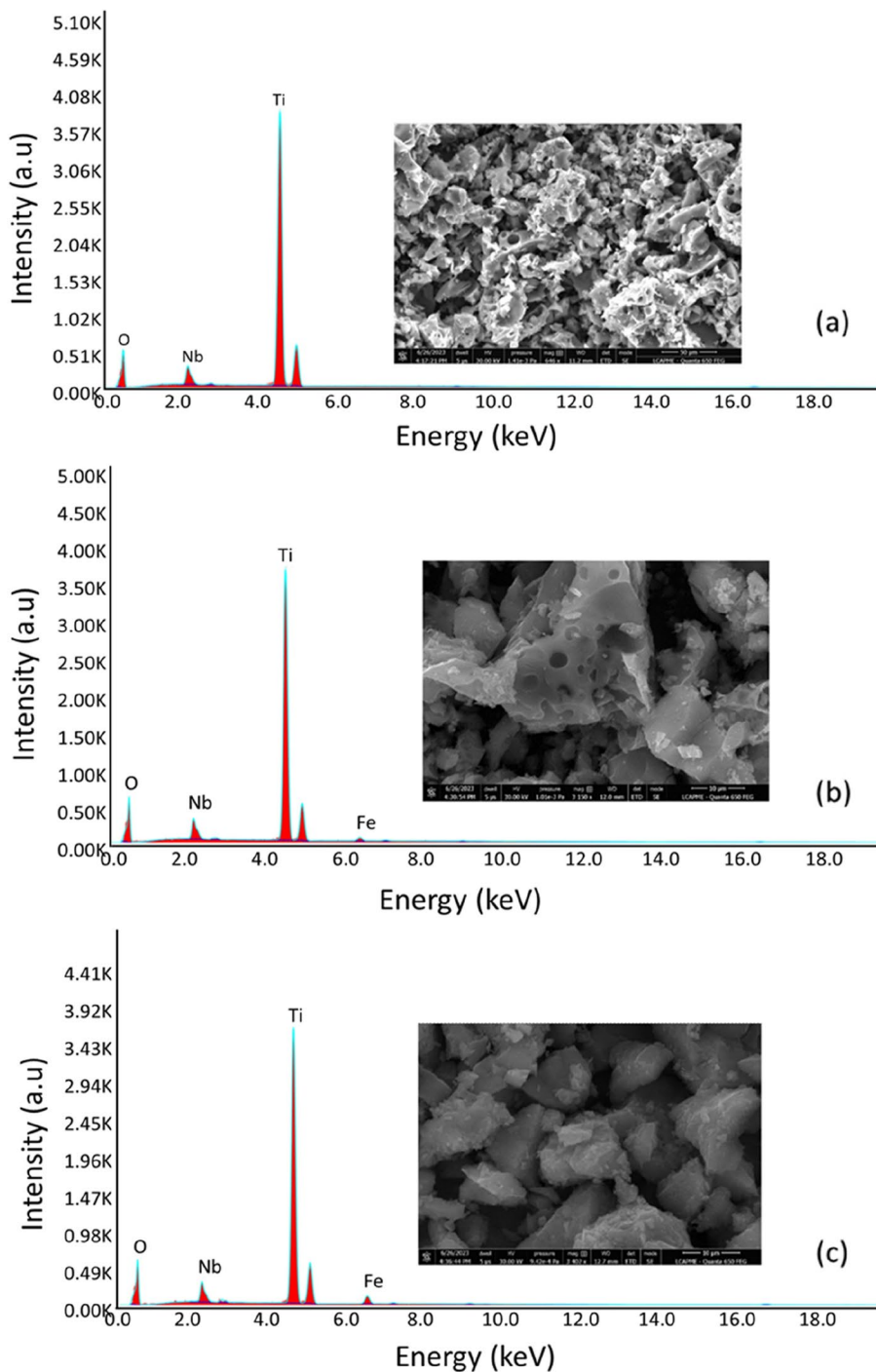

Fig. 3 SEM micrographs and EDX spectrum for different photocatalyst **a** P1, **b** P2, **c** P3

Lupu *et al. Sustainable Environment Research*   (2023) 33:36

Page 6 of 12
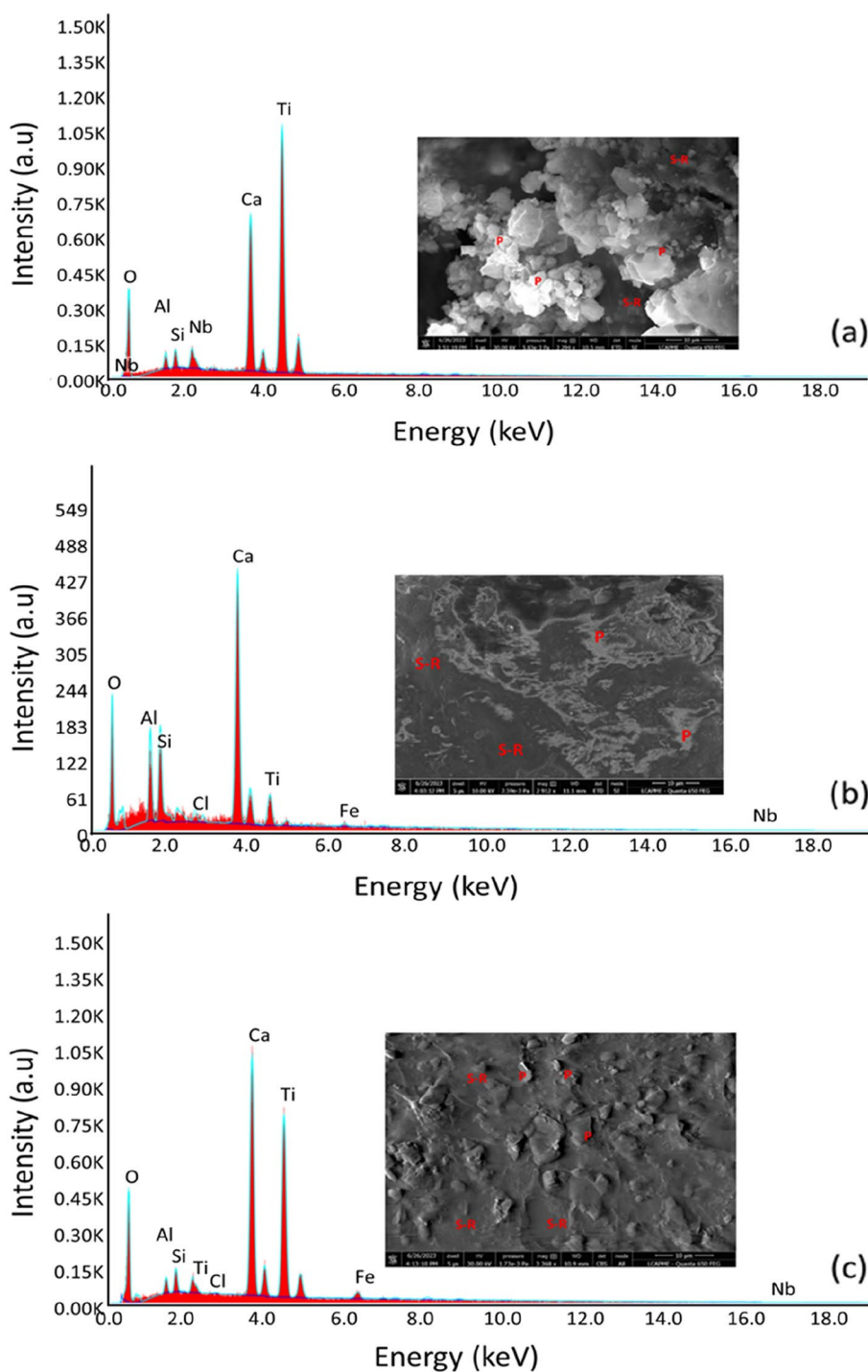
Fig. 4 SEM micrographs and EDX spectrum for photocatalytic membrane **a** M1, **b** M2, **c** M3

to Nb-O-Ti vibrations. The transmittance corresponding to 1529 cm^{-1} in P2 and P3 spectra could be attributed to Ti-O-Fe bound [25, 26]. Moreover, the band at approximately 1700 cm^{-1} cand be attributed to C=O,

most probably derived from the photocatalyst preparation method. Anatase phase of TiO$_2$ shows certain strong FTIR bands in the region of 1200–1300 cm^{-1}, where is seen the broad intense band attributed to Ti-O-Ti vibrations [27].
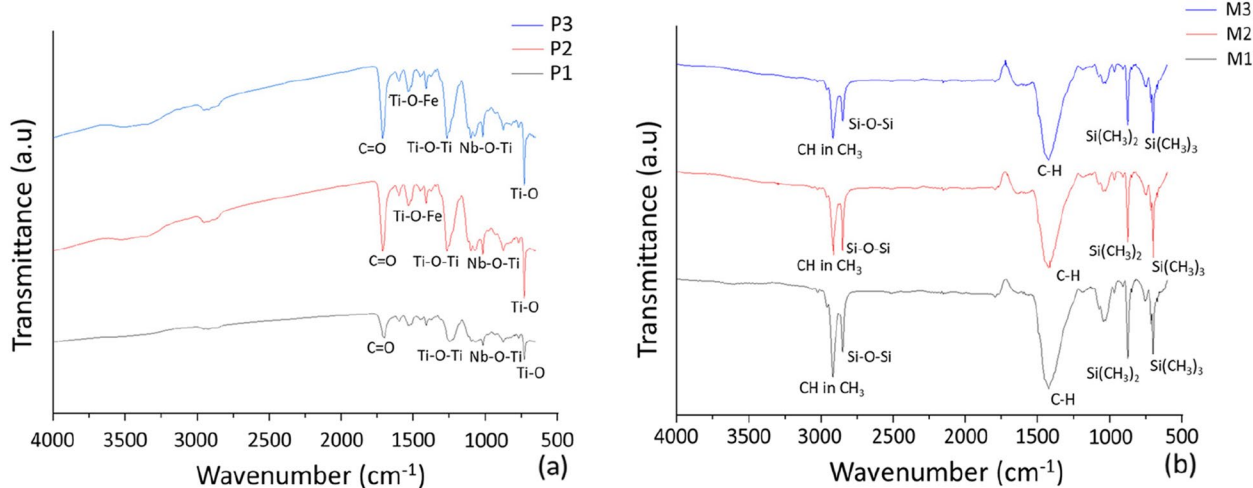
Fig. 5 FTIR spectra for the photocatalysts **a** initial photocatalysts, **b** photocatalytic membranes

The FTIR spectra for all the three photocatalytic membranes are shown in Fig. 5b. The peaks at approximately 700 cm^{-1} are corresponding to the functional groups Si-(CH$_3$)$_3$, and other peaks between 840–790 cm^{-1} can be attributed to Si-(CH$_3$)$_2$ functional groups. Peaks between 1100–1000 cm^{-1} correspond to Si-O-Si functional groups [28, 29]. All these functional groups show the presence of silicone rubber in the composition of new obtained photocatalytic membranes [30]. Other peaks at 2960 cm^{-1} show the presence of CH stretch in CH$_3$ functional group.

3.5 X-ray Photoelectron Spectroscopy

Figure 6a shows the XPS full spectra of the photocatalysts P1-P3. For the photocatalyst P1, the peaks at 207.3 and 458.8 eV are corresponding to Nb 3d (Nb 3d$_{5/2}$) and Ti 2p (Ti 2p$_{3/2}$). Nb 3d$_{3/2}$ peak corresponds to that of Nb^{5+} oxidation state, and Ti 2p$_{3/2}$ peak corresponds to that of Ti^{4+} oxidation state [31]. For photocatalysts P2 and P3, the peaks that appear at approximately 710 eV correspond to the added iron (Fe2p). The deconvolution of these peaks (Fig. 6b and c) showed that the Fe 2p$_{3/2}$ peaks correspond to the Fe^{2+} (709 eV) and Fe^{3+} (711 and 712 eV) oxidation states. The O 1s peak corresponds to the lattice oxygen of TiO$_2$ [32].

Figure 7 shows the full spectra of the photocatalytic membranes. It should be noted that the XPS analysis for the three photocatalytic membranes was performed after 2 h of UV irradiation. It seems that the peaks corresponding to titanium (Ti 2p at 458.8 eV) and niobium (Nb 3d$_{3/2}$ at 210.2 eV) appear in the spectra of the three photocatalytic membranes, but at a reduced intensity compared to the initial spectra

of photocatalysts. This denotes a good stability of the photocatalytic membranes, which would allow their use in several successive cycles of photocatalysis. Regarding the peak associated with iron, it is shifted to 219.2 eV corresponding to Fe2p$_{1/2}$, thus indicating the complete transition to Fe^{3+} in γ-Fe$_2$O$_3$ after UV irradiation.

3.6 Photocatalytic degradation experiments

3.6.1 Initial photocatalytic tests

The initial photocatalytic tests (membrane without addition of organic material) showed that the photocatalytic membranes are stable, the concentration of organic material in the solution, which would have come strictly from the composition of the membranes, was zero. Also, the photocatalyst embedded in the membranes was not released into the solution, which confirms its physical stability.

3.6.2 Photocatalytic degradation tests

The results obtained using the M1 membrane (Fig. 8a) indicate a fast degradation of the organic substrate (AZT + excipients) in the first 15 min of UV irradiation. The photocatalytic degradation follows a pseudo-first order kinetics whose rate constant over the interval 0–15 min is 0.054 min^{-1}. After 15 min of UV irradiation, the degradation of the remaining organic substrate continues, but at a very low rate, the rate constant for the interval 15–120 min being 0.0010 min^{-1}.

For M2 photocatalytic membrane (Fig. 8b), the experimental results obtained indicate a good degradation of the organic substrate in the first minutes (0–15 min) of
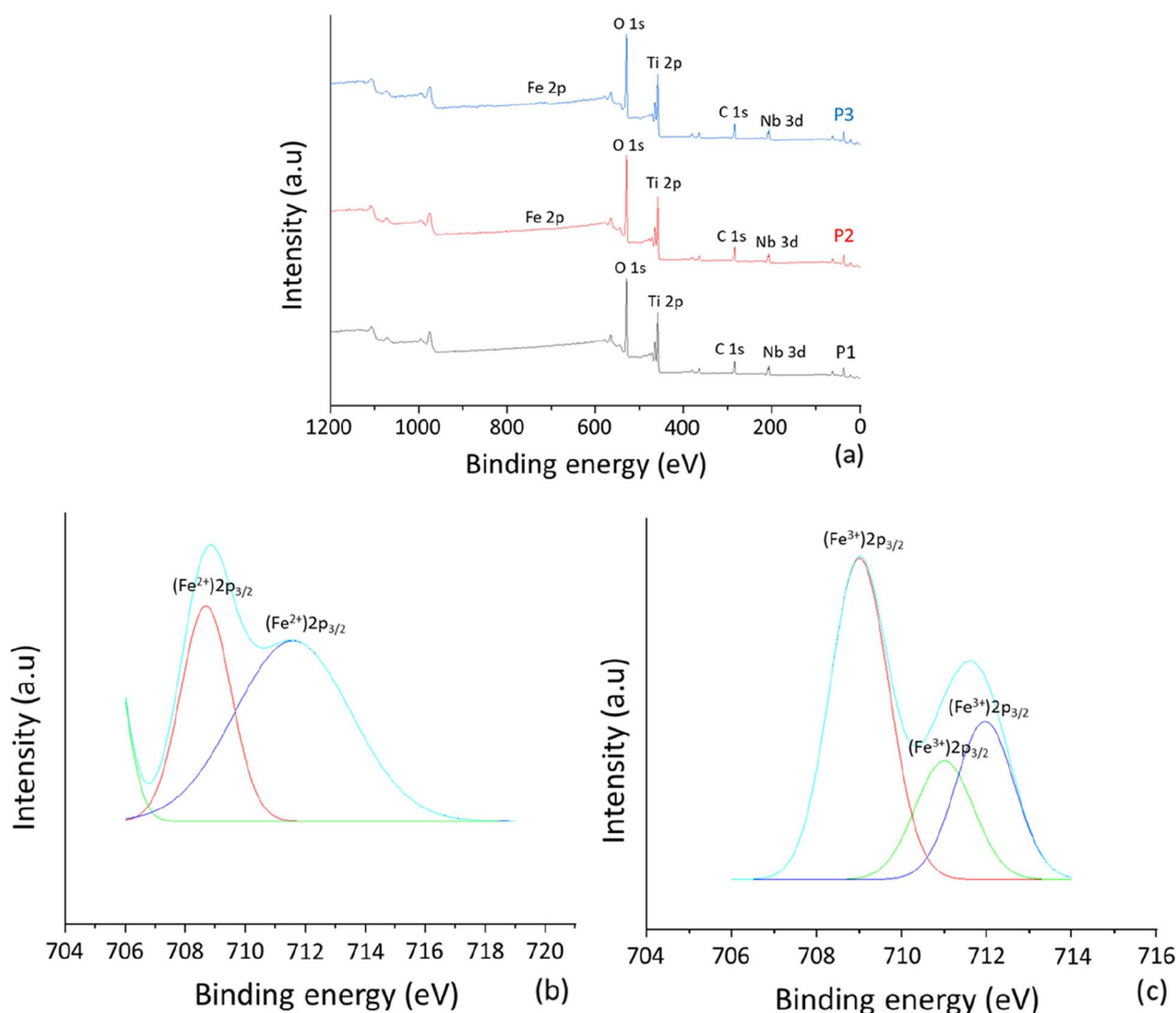
Fig. 6 XPS spectra of photocatalysts **a** full spectra of photocatalyst P1-P3, **b** deconvolution of Fe2p spectra in P2, **c** deconvolution of Fe2p spectra in P3

the UV irradiation. The process of photocatalytic degradation is following a pseudo-first order kinetics which in the first 15 min has a rate constant of 0.027 min^{-1}. In the next irradiation time (15–120 min), the rate constant is 0.0046 min^{-1}. Regarding the M3 photocatalytic membrane (Fig. 8c), the degradation, also follows a pseudo-first order kinetics, but the degradation rate is higher than in the case of the M2 membrane. Thus, on the interval 0–15 min the rate constant is 0.075 min^{-1}, and on the interval 15–120 min the rate constant is 0.0013 min^{-1}.

It can be observed that, in all the three cases, the degradation of the organic substrate proceeds in two steps, namely, a first step that proceeds at a high rate

over a short irradiation interval, and a second step that proceeds at a low rate over a long irradiation interval. This could be due to the high rate of degradation of the initial organic substrate to intermediate compounds with higher resistance to the photocatalytic oxidation conditions in the reactor. Taking into account that the degradation efficiency is about 60% in the case of the M1 membrane, over 63% in case of the M2 membrane and over 70% in the case of the M3 membrane, it can be concluded that most of the initial organic substrate is photocatalytically degraded in the first 15 min of irradiation, following as the degradation efficiency to increase slowly with the increase of the irradiation time of the intermediate compounds formed.
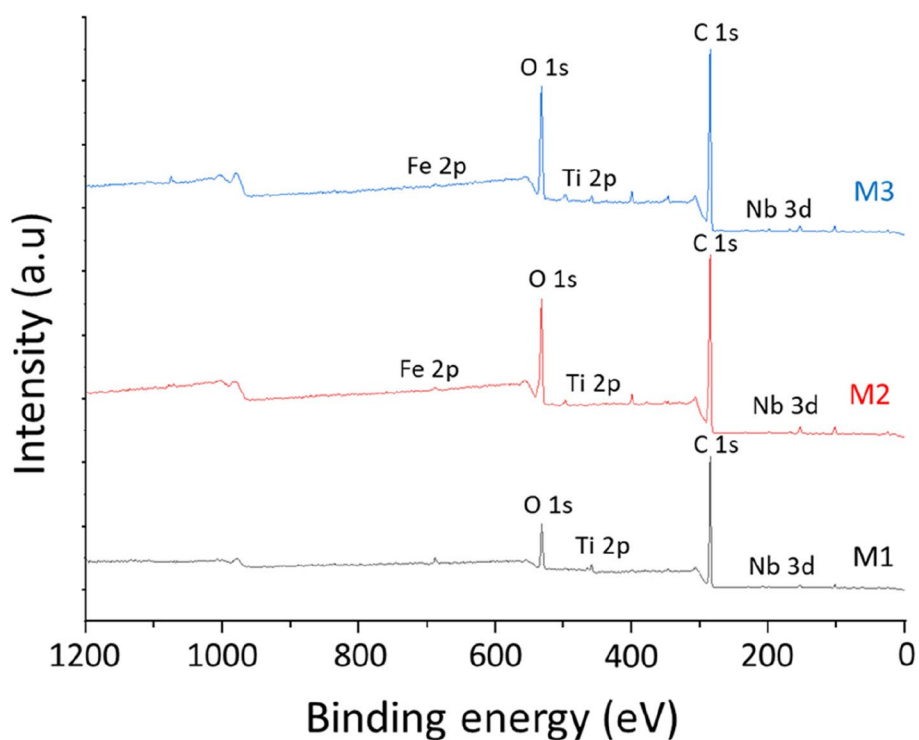
Fig. 7 XPS spectra of the photocatalytic membranes M1-M3
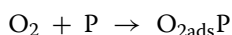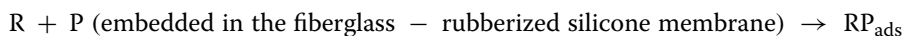
3.6.3 *The mechanism of photocatalytic degradation*

Considering that Langmuir-Hinshelwood photooxidation mechanism is valid for this case [33], the most probable action mechanism of these photocatalytic membranes is as follows:
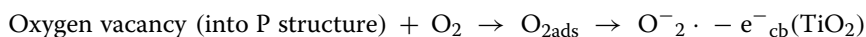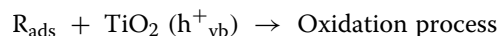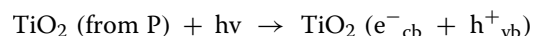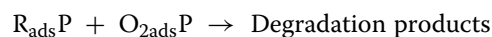
1. *Adsorption of organic material (R) and oxygen (O$_2$), generated in the system by means of oxygen peroxide, on the surface of the photocatalyst (P).*

$$R + P \text{ (embedded in the fiberglass } - \text{ rubberized silicone membrane)} \rightarrow RP_{ads}$$

$$O_2 + P \rightarrow O_{2ads}P$$

The presence of niobium in the structure of the photocatalyst favors the adsorption of O$_2$ due to the oxygen vacancies present in its structure. Thus, the formation of reactive O$^-_2\bullet$ species on the surface of the catalyst is accelerated, triggering the chain of reactions described below.
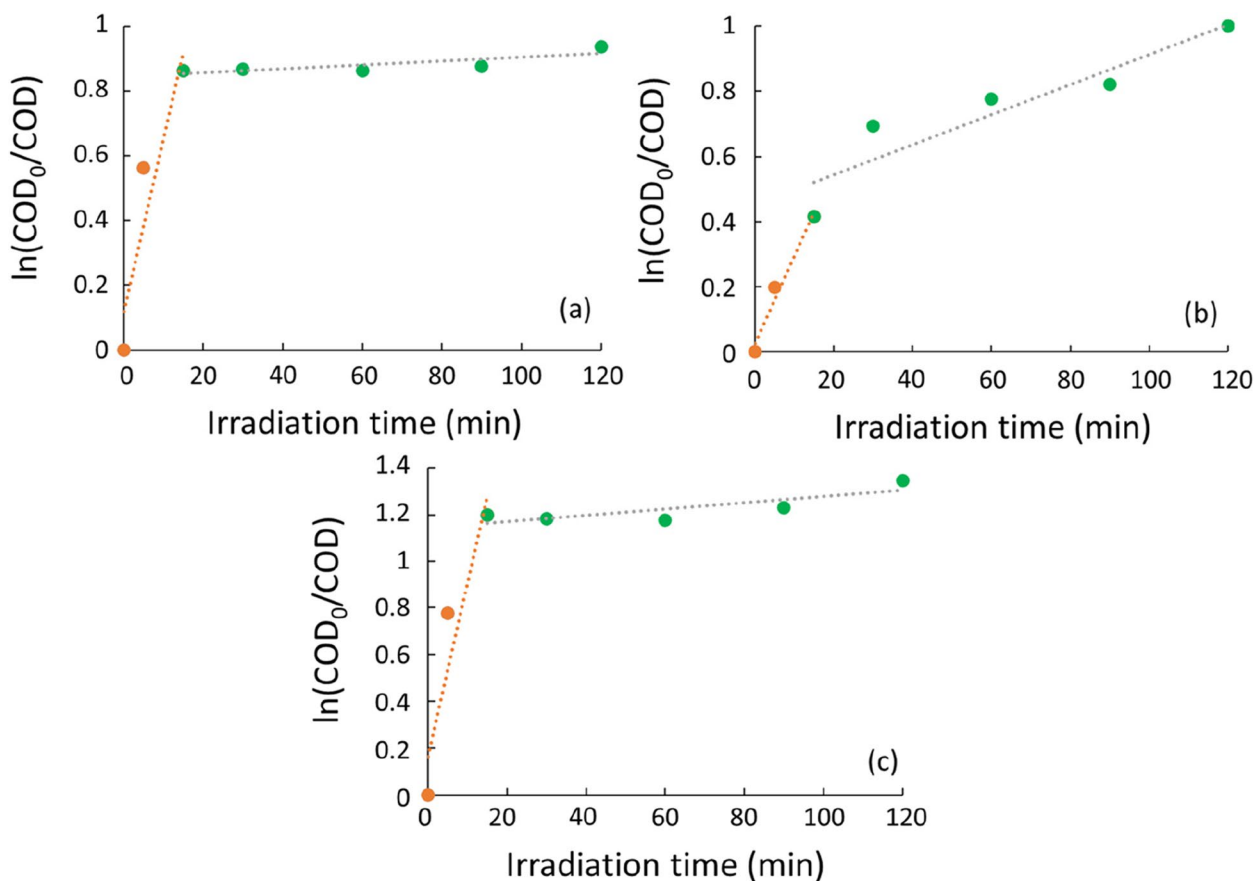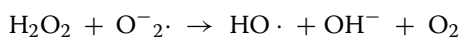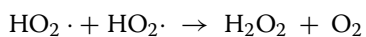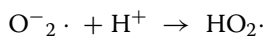
$$\text{Oxygen vacancy (into P structure)} + O_2 \rightarrow O_{2ads} \rightarrow O^-_2 \cdot - e^-_{cb}(TiO_2)$$

Also, the addition of niobium leads to the increase of the specific surface of the photocatalyst almost twice (from 94 to 164 m^2 g^{-1}), which contributes to the increase of its photocatalytic degradation efficiency.

2. *Photocatalytic degradation of the organic material (R) according to the following photocatalytic reaction mechanism at the surface of semi-conductors (TiO$_2$):*

$$R_{ads}P + O_{2ads}P \rightarrow \text{Degradation products}$$

$$TiO_2 \text{ (from P)} + hv \rightarrow TiO_2 (e^-_{cb} + h^+_{vb})$$

$$R_{ads} + TiO_2 (h^+_{vb}) \rightarrow \text{Oxidation process}$$

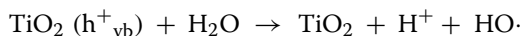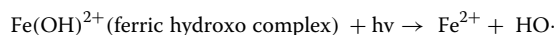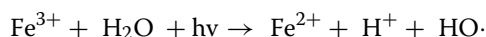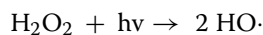**Fig. 8** Kinetics of the photocatalytic degradation of the azithromycin formulation by using different photocatalytic membranes **a** Membrane M1, **b** membrane M2, **c** membrane M3

$$TiO_2\ (h^+_{vb})\ +\ H_2O\ \rightarrow\ TiO_2\ +\ H^+\ +\ HO\cdot$$

$$TiO_2(h^+_{vb})\ +\ OH^-\ \rightarrow\ TiO_2\ +\ HO\cdot$$

$$R_{ads}\ +\ TiO_2(e^-_{cb})\ \rightarrow\ Reduction\ process$$

$$TiO_2(e^-_{cb})\ +\ O_{2ads}\ \rightarrow\ TiO_2\ +\ O^-_2\cdot$$

$$O^-_2\cdot\ +\ H^+\ \rightarrow\ HO_2\cdot$$

$$HO_2\cdot +\ HO_2\cdot\ \rightarrow\ H_2O_2\ +\ O_2$$

$$H_2O_2\ +\ O^-_2\cdot\ \rightarrow\ HO\cdot\ +\ OH^-\ +\ O_2$$

$$R_{ads}\ +\ HO\cdot\ \rightarrow\ Degradation\ products$$
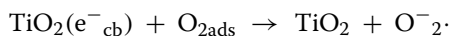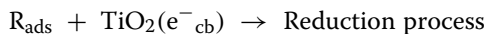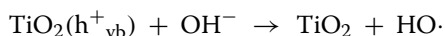
where: e^-_{cb} – electrons in the conduction band, h^+_{vb} – positive holes in the valence band, $O^-_2\bullet$ – superoxide radical, and $HO_2\bullet$ – hydroperoxyl radical. Photo-Fenton mechanism is added due to the presence of iron (Fe^{3+}) in the structure of the photocatalyst:

$$H_2O_2\ +\ hv \rightarrow\ 2\ HO\cdot$$

$$Fe^{3+}\ +\ H_2O\ +hv\ \rightarrow\ Fe^{2+}\ +\ H^+\ +\ HO\cdot$$

$$Fe(OH)^{2+}(ferric\ hydroxo\ complex)\ +hv\ \rightarrow\ Fe^{2+}\ +\ HO\cdot$$

$$R_{ads}\ +\ HO\cdot\ \rightarrow\ Degradation\ products$$

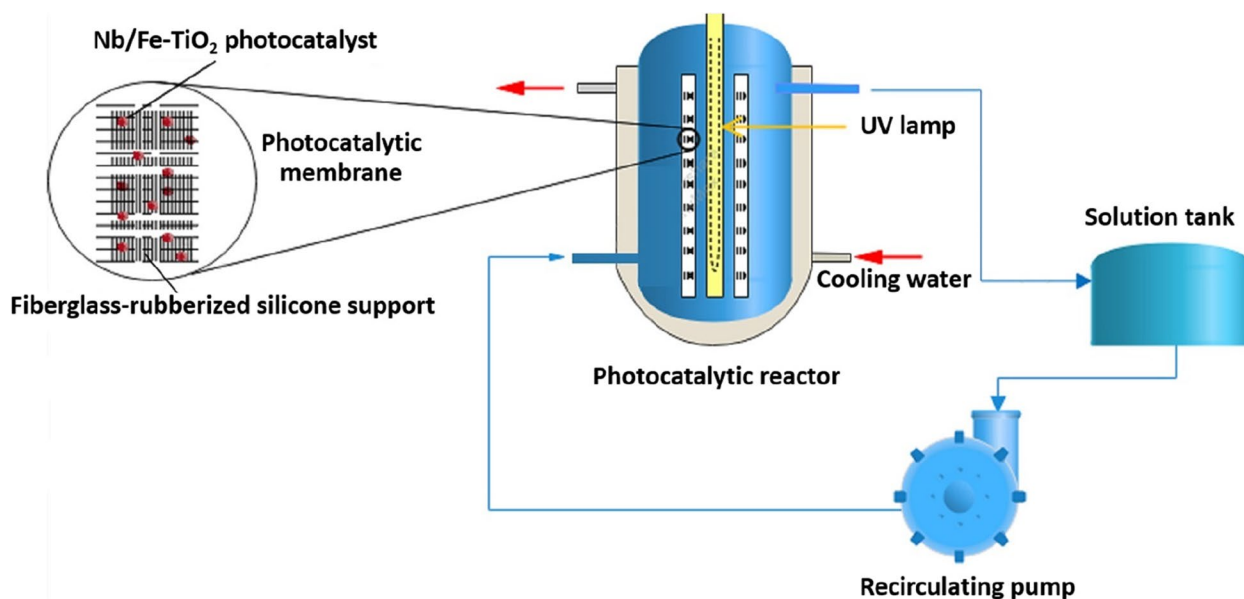where $Fe(OH)^{2+}$ is a ferric hydroxo complex.

Fig. 9 Schematic presentation of the photocatalytic degradation process

The whole process is shown schematically in Fig. 9.

4 Conclusions

The main original findings of this work are the following:

1. The successful insertion of niobium and iron into the structure of titanium dioxide, which led to an almost two-fold increase in its specific surface area, thus facilitating the course of the photocatalytic process.

2. The introduction of iron into the structure of the photocatalyst leads to the triggering of the photo Fenton degradation mechanism of the organic material, which leads to an increase in the global efficiency of the photocatalytic degradation process.

3. The fiberglass/rubberized silicone support in which the photocatalyst is embedded has high mechanical and physical-chemical resistance, which makes it ideal for making photocatalytic membranes on a large scale. It has great elasticity, thus being able to take different forms in the photocatalytic reactor without the risk of losing the photocatalyst from the surface or inside it, and it is practically inert in the strongly oxidizing conditions in the reactor.

Authors' contributions
Conceptualization, G.I.L. and C.B.; methodology, C.O. and C.B.; investigations, L.B., G.I.L., C.P., R.G.I., E.S.L., J.P.C. and M.N.V.; writing—original draft preparation, G.I.L., C.B. and C.O. All authors reviewed and edited the article. All authors read and approved the final manuscript.

Availability of data and materials
Data are available upon request.

Declarations

Competing interests
The authors declare they have no competing interests.

References
1. Firth A, Prathapan P. Azithromycin: The first broad-spectrum therapeutic. Eur J Med Chem. 2020;207:112739.
2. Parnham MJ, Haber VE, Giamarellos-Bourboulis EJ, Perletti G, Verleden GM, Vos R. Azithromycin: mechanisms of action and their relevance for clinical applications. Pharmacol Therapeut. 2014;143:225–45.
3. Al-Jaaf HJ, Ali NS, Alardhi SM, Albayati TM. Implementing eggplant peels as an efficient bio-adsorbent for treatment of oily domestic wastewater. Desalin Water Treat. 2022;245:226–37.
4. Abou Assi R, Darwis Y, Abdulbaqi IM, Asif SM. Development and validation of a stability-indicating RP-HPLC method for the detection and quantification of azithromycin in bulk, and self-emulsifying drug delivery system (SEDDs) formulation. J Appl Pharm Sci. 2017;7:20–9.
5. Imanipoor J, Mohammadi M, Dinari M, Ehsani MR. Adsorption and desorption of amoxicillin antibiotic from water matrices using an effective

Lupu *et al. Sustainable Environment Research*   (2023) 33:36

Page 12 of 12

and recyclable MIL-53(Al) metal–organic framework adsorbent. J Chem Eng Data. 2021;66:389–403.

6. Kadhum ST, Alkindi GY, Albayati TM. Determination of chemical oxygen demand for phenolic compounds from oil refinery wastewater implementing different methods. Desalin Water Treat. 2021;231:44–53.

7. Bote ME. Studies on electrode combination for COD removal from domestic wastewater using electrocoagulation. Heliyon. 2021;7:e08614.

8. Modabberasl A, Pirhoushyaran T, Esmaeili-Faraj SH. Synthesis of $CoFe_2O_4$ magnetic nanoparticles for application in photocatalytic removal of azithromycin from wastewater. Sci Rep-Uk. 2022;12:19171.

9. Abbood NS, Ali NS, Khader EH, Majdi HS, Albayati TM, Saady NMC. Photocatalytic degradation of cefotaxime pharmaceutical compounds onto a modified nanocatalyst. Res Chem Intermediat. 2023;49:43–56.

10. Wang H, Li X, Zhao X, Li C, Song X, Zhang P, et al. A review on heterogeneous photocatalysis for environmental remediation: From semiconductors to modification strategies. Chinese J Catal. 2022;43:178–214.

11. Subramaniam MN, Goh PS, Kanakaraju D, Lim JW, Lau WJ, Ismail AF. Photocatalytic membranes: a new perspective for persistent organic pollutants removal. Environ Sci Pollut R. 2022;29:12506–30.

12. Nasrollahi N, Ghalamchi L, Vatanpour V, Khataee A. Photocatalytic-membrane technology: a critical review for membrane fouling mitigation. J Ind Eng Chem. 2021;93:101–16.

13. Ali NS, Kalash KR, Ahmed AN, Albayati TM. Performance of a solar photocatalysis reactor as pretreatment for wastewater via UV, UV/TiO_2, and UV/H_2O_2 to control membrane fouling. Sci Rep-Uk. 2022;12:16782.

14. Dijkstra MFJ, Michorius A, Buwalda H, Panneman HJ, Winkelman JGM, Beenackers AACM. Comparison of the efficiency of immobilized and suspended systems in photocatalytic degradation. Catal Today. 2001;66:487–94.

15. Singh S, Mahalingam H, Singh PK. Polymer-supported titanium dioxide photocatalysts for environmental remediation: A review. Appl Catal A-Gen. 2013;462–463:178–95.

16. Silva MJ, Gomes J, Ferreira P, Martins RC. An overview of polymer-supported catalysts for wastewater treatment through light-driven processes. Water. 2022;14:825.

17. Bobirica C, Bobirica L, Rapa M, Matei E, Predescu AM, Orbeci C. Photocatalytic degradation of ampicillin using PLA/TiO_2 hybrid nanofibers coated on different types of fiberglass. Water. 2020;12:176.

18. APHA. Standard Methods for the Examination of Water and Wastewater. 18th ed. Washington, DC: American Public Health Association; 1992.

19. Ye L, Mao J, Liu J, Jiang Z, Peng T, Zan L. Synthesis of anatase TiO_2 nanocrystals with {101}, {001} or {010} single facets of 90% level exposure and liquid-phase photocatalytic reduction and oxidation activity orders. J Mater Chem A. 2013;1:10532.

20. Pai R, Singh A, Simotwo S, Kalra V. In situ grown iron oxides on carbon nanofibers as freestanding anodes in aqueous supercapacitors. Adv Eng Mater. 2018;20:1701116.

21. Santos KMA, Albuquerque EM, Coelho TL, Fraga MA. Continuous aqueous-phase cascade conversion of trioses to lactic acid over Nb_2O_5 catalysts. Biomass Convers Bior. 2023;13:11865–78.

22. Shannon RD. Revised effective ionic radii and systematic studies of interatomic distances in halides and chalcogenides. Acta Crystallogr A. 1976;32:751–67.

23. Heracleous E, Lemonidou AA. Ni–Nb–O mixed oxides as highly active and selective catalysts for ethene production via ethane oxidative dehydrogenation. Part I: Characterization and catalytic performance. J Catal. 2006;237:162–74.

24. Neto AdBS, Oliveira AC, Mishra S, Essayem N. Sol-Gel controlled dispersion of Nb within TiO_2 to obtain water tolerant catalysts with tunable acid-base properties for dihydroxyacetone transformation. Appl Catal A-Gen. 2023;658:119165.

25. Lü X, Mou X, Wu J, Zhang D, Zhang L, Huang F, et al. Improved-performance dye-sensitized solar cells using Nb-doped TiO_2 electrodes: Efficient electron injection and transfer. Adv Funct Mater. 2010;20:509–15.

26. Kokorin AI, Amal R, Teoh WY, Kulak AI. Studies of nanosized iron-doped TiO_2 photocatalysts by spectroscopic methods. Appl Magn Reson. 2017;48:447–59.

27. Ganesh I, Kumar PP, Gupta AK, Sekhar PSC, Radha K, Padmanabham G, et al. Preparation and characterization of Fe-doped TiO_2 powders for solar light response and photocatalytic applications. Process Appl Ceram. 2012;6:21–36.

28. Kumara V, Kumar A, Chhatra RK, Lee DL. Studies on high performance rubber composites by incorporating titanium dioxide particles with different surface area and particle size. Nanofabrication. 2022;7:104–15.

29. Wang Z, Zhang X, Wang F, Lan X. Chemical characterization and research on the silicone rubber material used for outdoor current transformer insulation. Phosphorus Sulfur. 2017;192:109–12.

30. Vangapandu DN, Paul M, Mishra P, Sarathi R, Paramane A, Nazir MT. Performance evaluation of thermally aged RTV silicone rubber/TiO_2 nanocomposites in mineral oil for transformer bushings. IEEE T Dielect El In. 2023;30:1493–501.

31. Kaleji BK, Sarraf-Mamoory R, Fujishima A. Influence of Nb dopant on the structural and optical properties of nanocrystalline TiO_2 thin films. Mater Chem Phys. 2012;132:210–5.

32. Ruzgar S, Pehlivanoglu SA. The effect of Fe dopant on structural, optical properties of TiO_2 thin films and electrical performance of TiO_2 based photodiode. Superlattice Microst. 2020;145:106636.

33. Bobirica L, Bobirica C, Lupu GI, Orbeci C. Influence of operating parameters on photocatalytic oxidation of 2,4-dichlorofenol in aqueous solution by TiO_2/stainless steel photocatalytic membrane. Appl Sci. 2021;11:11664.

Publisher's Note